Particle-hole-symmetric model for a paired fractional quantum Hall state in a half-filled Landau level

William Hutzel,[1] John J. McCord,[1] P. T. Raum,[2] Ben Stern,[2] Hao Wang,[3] V. W. Scarola,[2] and Michael R. Peterson[1,4]

[1]*Department of Physics & Astronomy, California State University Long Beach, Long Beach, California 90840, USA*
[2]*Department of Physics, Virginia Tech, Blacksburg, Virginia 24061, USA*
[3]*Shenzhen Institute for Quantum Science and Engineering, and Department of Physics, Southern University of Science and Technology, Shenzhen 518055, China*
[4]*Kavli Institute for Theoretical Physics, University of California, Santa Barbara, California 93106, USA*

The fractional quantum Hall effect (FQHE) observed at half filling of the second Landau level is believed to be caused by a pairing of composite fermions captured by the Moore-Read Pfaffian wave function. The generating Hamiltonian for the Moore-Read Pfaffian is a purely three-body model that breaks particle-hole symmetry and lacks other properties, such as dominate two-body repulsive interactions, expected from a physical model of the FQHE. We use exact diagonalization to study the low-energy states of a more physical two-body generator model derived from the three-body model. We find that the two-body model exhibits the essential features expected from the Moore-Read Pfaffian: pairing, non-Abelian anyon excitations, and a neutral fermion mode. The model also satisfies constraints expected for a physical model of the FQHE at half-filling because it is short range, spatially decaying, particle-hole symmetric, and supports a roton mode with a robust spectral gap in the thermodynamic limit. Hence, this two-body model offers a bridge between artificial three-body generator models for paired states and the physical Coulomb interaction and can be used to further explore properties of non-Abelian physics in the FQHE.

I. INTRODUCTION

Soon after the construction of the Laughlin wave functions [1] for the FQHE [2] at electronic filling factors $\nu = 1/(2p + 1)$ (p an integer), a short-range generator Hamiltonian [3,4] was found that produced the Laughlin wave functions as unique gapped ground states. This model shared properties of the Coulomb interaction: It is two-body, consists of interactions decaying with distance, and is invariant under particle-hole (PH) transformations. Moreover, the model was shown to generate states that accurately described the experimentally observed FQHE at filling factors $\nu = n_0/(2pn_0 \pm 1)$ (for integer n_0) in the lowest Landau level (LLL). In fact, the ground states of this generator model are virtually identical to the composite fermion (CF) wave functions [5,6] (the CF wave functions incorporate the Laughlin wave functions as a subset). The CF wave functions are written as $\mathcal{J}^{2p}\phi$, where the Jastrow factor $\mathcal{J}$ "binds" $2p$ vortices of the many-body wave function to electrons described by ϕ. This strongly interacting *electron* wave function $\mathcal{J}^{2p}\phi$ is interpreted as a wave function for CFs described only by ϕ. The choice $\phi \rightarrow \phi_{n_0}$ describes CFs completely filling n_0 CF LLs and yields low-energy wave functions with the same quantum numbers and physics of the low-energy states of the generator model, the Coulomb interaction in the lowest LL, and importantly describes the FQHE at filling factor $\nu = n_0/(2pn_0 \pm 1)$. These wave functions (and generator model) also predict a gapless PH-symmetric state at half-filling described as a CF-Fermi sea ($\phi \rightarrow \phi_{FS}$) [7–10] that accurately captures the physics of the Coulomb interaction at half-filling of the LLL [6,11].

The unexpected discovery of the FQHE in the half-filled second LL [12] (total filling factor 5/2) led to the construction of the gapped Moore-Read Pfaffian state at half-filling [13]. This state can be interpreted as a paired state of CFs [14,15], written via $\phi \rightarrow \phi_{BCS}$ where ϕ_{BCS} is a Bardeen-Cooper-Schrieffer state of CFs (a Pfaffian in real space) pairing CFs in the p-wave channel [13,16]. Wave functions of this type are excellent candidates for the FQHE at filling factor 5/2 [9,17–28] and predict non-Abelian quasiparticles [13,29–32], which, if identified experimentally, could form building blocks in the construction of a topologically protected quantum computer [33,34].

Interestingly, a purely repulsive three-body generator Hamiltonian [35] (labeled H_3) yields most of the physics described by Moore and Read [13]. Specifically, H_3 generates the Moore-Read Pfaffian wave function as an exact ground state and produces a degenerate manifold of non-Abelian quasihole excitations [36]. But H_3 does not obey *all* the properties expected of a *physical* model of the FQHE at half-filling. First, the model does not respect PH-symmetry. This constraint might not be crucial since numerical work indicates the ground state of the Coulomb interaction in the half-filled second LL breaks PH-symmetry [37] with additional PH-symmetry breaking terms. Importantly, LL-mixing effects in realistic models supply emergent PH-symmetry breaking three-body terms [38–42]. Second, H_3 is purely three-body, challenging theory to bridge it to physical two-body models since additional two-body terms added to H_3 generally lift [18,23,37,43] expected degeneracies [36]. The

construction of H_3 is constrained by the Pfaffian form of ϕ_{BCS} but other forms [16] could yield states and generator models satisfying all physical requirements while potentially preserving topological properties including non-Abelian anyon excitations.

The authors of Ref. [44] discovered that H_3 can be added to its PH conjugate Hamiltonian $\overline{H}_3$ (which generates the anti-Pfaffian [45,46]) to yield a purely *two-body* model:

$$H_2 = H_3 + \overline{H}_3. \tag{1}$$

H_2 has all of the properties desired of a physical model: It is two-body, PH-symmetric, and spatially decays with distance. Furthermore, the ground-state energy of H_2, as a function of particle number, displays a "wine bottle" potential structure, interpreted originally as evidence for spontaneous PH-symmetry breaking in the ground state. Subsequent work showed the ground-state energies have a prominent even-odd effect [47] indicative of pairing. These properties are consistent with the model's definition in terms of generators for the Moore-Read Pfaffian/anti-Pfaffian. However, many important aspects of H_2 remain unexplored as a stand-alone generator model for FQHE at half-filling of a single LL.

In this work we use numerical exact diagonalization to show that H_2 offers a more physical generator model for the FQHE at half-filling that shares essential features of the generator model of the Moore-Read Pfaffian including a spectral gap at half-filling with a neutral roton mode [48,49]. When combined with the fact that H_2 is short ranged, PH-symmetric, and two-body, it becomes a useful generator model for half-filled FQHE states that connects the physical Coulomb interaction with the non-physical three-body generator model of the Moore-Read Pfaffian. We show that the low-energy states of H_2 are adiabatically connected to the Moore-Read Pfaffian, possess the same topological entanglement properties, and support (quasi)degenerate non-Abelian quasiparticles. We find conflicting evidence for spontaneous PH-symmetry breaking in the ground state of H_2. More work is needed to unambiguously determine if the ground state of H_2 spontaneously break PH-symmetry at half filling.

The paper is organized as follows. In Sec. II we define the two-body model, H_2, and show how it can be rewritten as a linear combination of three-body models. Section III examines the low-energy excitations and shows that H_2 supports a FQHE gap at half-filling in the thermodynamic limit. The roton mode and neutral fermion mode, expected from the Moore-Read Pfaffian, are shown to exist. Section IV tracks the low-energy excitations while tuning between H_2 and H_3. Here it is shown that all low-energy states are adiabatically connected and the low-energy manifold of H_2 possess (quasi)degenerate non-Abelian quasiholes consistent with Moore-Read Pfaffian expectations. Section V studies the PH-symmetry properties of the ground state of H_2. It is found that the ground states using the torus geometry do not appear to spontaneously break PH-symmetry, but further work is needed to conclusively establish this fact. Finally, Sec. VI shows that the ground and low-energy states have entanglement properties consistent with the Moore-Read Pfaffian. We summarize our results in Sec. VII.

II. MODEL

The two-body model we consider is a short-range model of N interacting spin-polarized fermions [50] confined to two-dimensions and the LLL:

$$H_2 = \sum_{i<j}^{N} \left[\hat{P}_{ij}(1) + \frac{1}{3}\hat{P}_{ij}(3) \right]$$
$$= \sum_{i<j<k}^{N} [\hat{P}_{ijk}(3) + \overline{\hat{P}}_{ijk}(3)], \tag{2}$$

where $\hat{P}_{ij}(m)$ denotes projection [3] onto two-body eigenstates of relative angular momentum m. Similarly, $\hat{P}_{ijk}(m)$ denotes projection onto the *three-body* eigenstates of relative angular momentum m. Here and in what follows, the overline denotes PH conjugation and we focus on half-filling. We work in energy units of the interaction strength and all distances are in units of the magnetic length.

The first line in Eq. (2) shows that H_2 is a repulsive two-body interaction that decays with interparticle separation. We can see this by noting that interparticle separation increases with m. More explicitly, the two-body projectors can be written in real-space in the disk geometry [4] as

$$\hat{P}_{ij}(m) = \nabla^{2m}\delta(r_{ij}), \tag{3}$$

where r_{ij} denotes the planar separation between particles i and j. The $m = 3$ term in Eq. (2) enforces repulsion at distances larger than the $m = 1$ term alone. At half-filling the $m = 1$ term, by itself, is known to generate the CF Fermi sea [6–8]. We show below the addition of the second $m = 3$ term leads to pairing. The prefactor of $1/3$ on the $m = 3$ term derives automatically from a re-expression of the two-body interaction as a sum of three-body interactions [44]. Appendix A discusses the Haldane pseudopotential expansion of H_2 for finite-sized spherical systems [3].

The second line in Eq. (2) shows the remarkable fact that a repulsive two-body interaction can be rewritten as the exact generator of CF paired states. $H_3 \equiv \sum_{i<j<k} \hat{P}_{ijk}(3)$ and $\overline{H}_3 \equiv \sum_{i<j<k} \overline{\hat{P}}_{ijk}(3)$ are Hamiltonians that generate the Moore-Read Pfaffian Ψ_{Pf} and its PH conjugate, the anti-Pfaffian $\Psi_{aPf} \equiv \overline{\Psi}_{Pf}$, respectively [more compactly written in Eq. (1)]. The equality in Eqs. (1) and (2) hold up to single particle terms that we have absorbed into a redefined chemical potential.

An important feature of H_2 is that it precisely connects the CF-Fermi sea [specifically ground states of $\sum_{i<j} \hat{P}_{ij}(1)$] with the Moore-Read Pfaffian. Over-screening of the inter-CF interaction can lead to a Kohn-Luttinger-type [51,52] instability in the CF-Fermi sea toward a CF paired state thereby favoring wave functions with ϕ_{BCS} over ϕ_{FS}. The CF wave functions themselves were shown to harbor their own instability in the p-wave channel when studied in the second LL [14]. In other words, H_2 shows that by adding $\hat{P}_{ij}(3)$ terms to the model that generates the CF-Fermi sea, a paired state is favored. At lowest-order, when electrons form CFs, the vortex binding accommodates the energy cost of the $\hat{P}_{ij}(1)$ term at short range. The addition of $\hat{P}_{ij}(3)$ terms can be interpreted
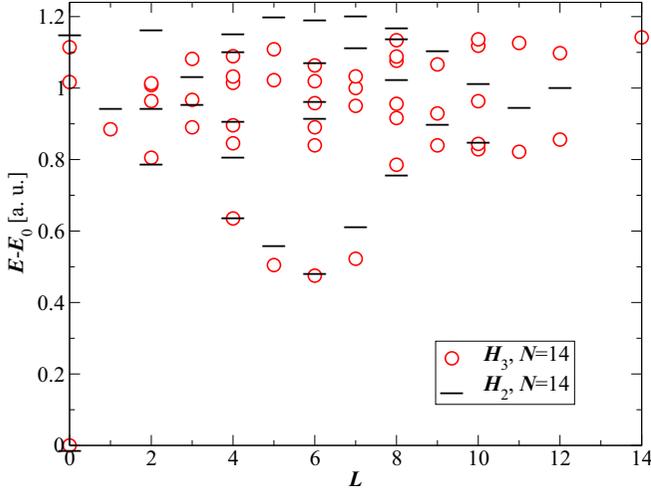
FIG. 1. Energy spectrum of the two-body model, H_2 (black dashes), and three-body model that generates the Moore-Read Pfaffian, H_3 (red circles), for $N = 14$ and $Q = 12.5$ on the sphere.

as forcing an over-screening of the $\hat{P}_{ij}(1)$ interaction terms leading to a pairing instability of the CF Fermi sea.

III. LOW-ENERGY EXCITATIONS AND THE ENERGY GAP

We begin our study of H_2 by addressing the FQHE energy gap using exact diagonalization in the spherical geometry [3]. Half-filling occurs for $N = (2Q + S)/2$ where $2Q$ is the total magnetic flux through the surface of a sphere of radius $R = \sqrt{Q}$ and S is the so-called shift, an order-one correction that vanishes in the thermodynamic limit [53]. The ground state of H_3 ($\overline{H}_3$) is Ψ_{Pf} (Ψ_{aPf}) at a shift of $S = 3$ ($S = -1$). A gap is necessary for the ground state of H_2 at $2Q = 2N - S$ to represent a valid FQH state. Hence, we calculate the low-energy spectrum of H_2 (shown for $N = 14$ in Fig. 1 and in Ref. [44] for $N = 8$) and define the gap as the difference between the energy of the first excited state and the $L = 0$ ground state (if the ground state has $L \neq 0$ then the gap is take to be zero). Ψ_2 is found to be a uniform state with total angular momentum $L = 0$ separated from excited states by a finite gap, Δ_{Ψ_2}. In fact, the structure of the low-energy spectrum is notably similar to the low-energy spectrum of the second LL Coulomb interaction and H_3 [44]. We also calculate the thermodynamic limit of the energy gap between the first excited state and the $L = 0$ ground state— the so-called "roton" gap. From Fig. 2 we see the gap is finite and nearly identical in the thermodynamic limit to the Moore-Read Pfaffian gap, $\Delta_{\Psi_{Pf}}$ [23].

The Moore-Read Pfaffian state additionally supports a so-called neutral fermion mode [13,16,48,54], which we can study in H_2 as well. Following Ref. [48] we calculate the neutral fermion mode by considering a system at odd N and $2Q = 2N - 3$. To define the neutral gap we construct a "ground-state" energy at odd N by finding the linear interpolation between the ground-state energy of the nearby even particle systems at $N + 1$ and $N - 1$ (again for $2Q = 2N - 3$).
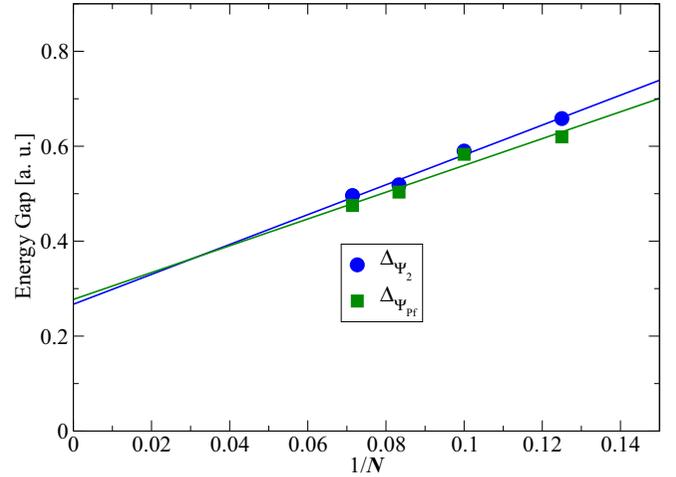

FIG. 2. Energy gap between the lowest energy excited state and the uniform ground state of H_2 (denoted by Δ_{Ψ_2}) and H_3 (denoted $\Delta_{\Psi_{Pf}}$), respectively, as a function of inverse particle number. Linear extrapolations find the gaps in the thermodynamic limit to be $\Delta_{\Psi_2} = 0.267(24)$ and $\Delta_{\Psi_{Pf}} = 0.277(47)$. The numbers in parenthesis are the standard deviation in the linear extrapolation.

The neutral mode dispersion $\Delta_{NF}(k)$ of H_2 is shown in Fig. 3 and is remarkably similar, qualitatively and quantitatively, to the neutral mode of H_3.

IV. ADIABATIC CONTINUITY

To investigate whether Ψ_2 is indeed in the same universality class as the Moore-Read Pfaffian we consider the adiabatic continuity (or lack thereof) between the ground and low-energy states of H_2 to those of H_3. More concretely, we
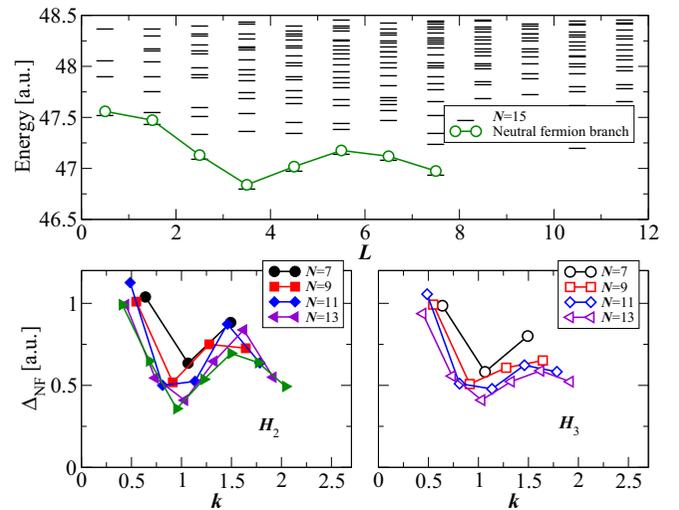

FIG. 3. The top panel shows the spectrum of H_2 for $N = 15$ at $2Q = 27$ and identifies the neutral fermion mode. The bottom panels show the neutral fermion modes for systems up to $N = 13$ for H_2 (left) and H_3 (right). These figures can be compared to those for H_3 and the second LL Coulomb Hamiltonian in Ref. [48]. The wave vector is $k = L/\sqrt{Q}$.
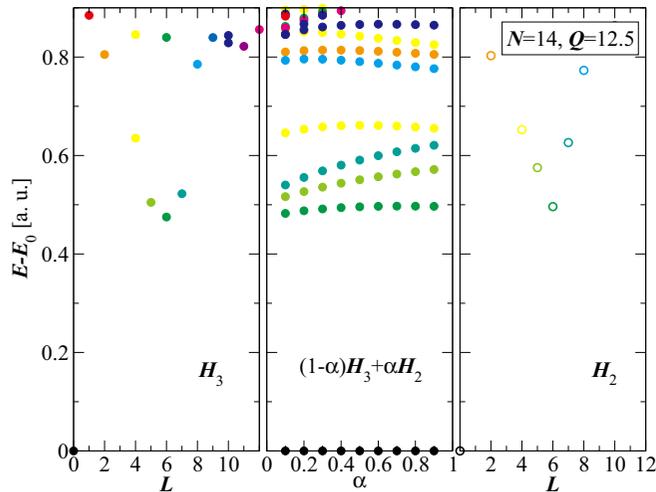
FIG. 4. Energy of $H(\alpha)$ relative to the ground state E_0. The middle panel shows the low-energy spectrum (lowest approximately 15 states) for $H(\alpha)$ as a function of α for $N = 14$ and $Q = 12.5$. The left and right panels plot relative energy as a function of angular momentum L for $\alpha = 0$ and 1, respectively. The angular momentum of each state is indicated by color. The gap stays open and relatively constant indicating adiabatic continuity.

consider the Hamiltonian

$$H(\alpha) = (1 - \alpha)H_3 + \alpha H_2 \qquad (4)$$

that interpolates between H_3 and H_2 for $\alpha \in [0, 1]$. Clearly, $H(0) = H_3$ and $H(1) = H_2$ where the ground states are Ψ_{Pf} and Ψ_2, respectively. As we tune α from zero to unity we track the ground state and energy gap. We denote the ground state(s) of $H(\alpha)$ as Ψ.

A. Adiabatic continuity in the ground state and neutral modes

We first consider the spherical geometry at $2Q = 2N - 3$ and investigate the ground states of $H(\alpha)$. For the two systems to be adiabatically connected we expect the spectrum to maintain a uniform ground state with $L = 0$ in addition to a finite gap Δ that smoothly interpolates between the two end points without vanishing. Otherwise, we expect the gap to close at some finite α_c indicating a quantum phase transition between Ψ_{Pf} and Ψ_2.

Figure 4 shows the low-energy spectrum for $H(\alpha)$ as a function of α for $N = 14$. The low-energy states of H_3 and H_2 are clearly adiabatically connected–the gap Δ between the first excited state and the ground state remains open and remarkably constant from $\alpha = 0$ to $\alpha = 1$. The absolute size of Δ for H_3 and H_2 are within 5% of one another at the end points. Furthermore, many of the higher-energy states (in the continuum) are also adiabatically connected. Smaller systems ($N = 12$, 10, and 8) show similar qualitative and quantitative results.

Figure 4 represents adiabatic continuity between Ψ_2 and Ψ_{Pf} for finite-sized systems (we have shown $N = 14$). However, to examine the effect of system size on the adiabatic continuity we calculate the linear extrapolation of the energy gap versus $1/N$, i.e., we take the thermodynamic limit, for
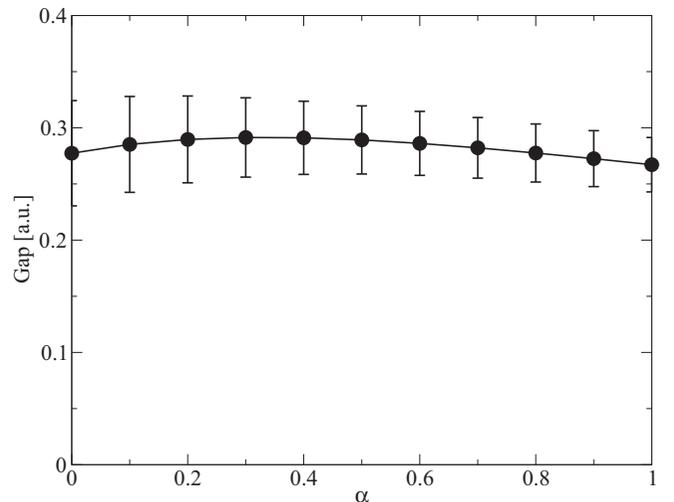

FIG. 5. The thermodynamic limit of the energy gap of $H(\alpha)$ is shown versus α. Similar to the finite-size system results of Fig. 4 the gap remains finite and largely flat, adiabatically connecting Ψ_2 with Ψ_{Pf}. The error bars indicate the standard deviation in the linear extrapolation.

several α between zero and one. Figure 5 shows the thermodynamic limit of Δ remains finite for all α and essentially reflects the finite-sized system results. The fact the system remains gapped in this limit further supports the conclusion that Ψ_2 and Ψ_{Pf} are in the same universality class.

We now use exact diagonalization on the torus to further investigate the low-energy states of $H(\alpha)$. We work with the rectangular unit cell with aspect ratio τ near unity and present results for system sizes with ground states at the total momenta consistent with pairing, i.e., the same ground-state momenta found for the ground states of H_3 (cf. Refs. [18,55]). The upper two panels of Fig. 6 show the low-energy spectrum of $H(\alpha)$ for $N = 8$ and $N = 12$ with $\tau = 0.95$ (our results are robust to changes in τ). In this geometry the topological order of the Moore-Read Pfaffian state is in evidence by the existence of a three-fold ground-state degeneracy separated from the higher-energy continuum by a gap. As α is tuned from H_3 to H_2 we see that, while the three-fold ground-state degeneracy is minimally broken due to "tunneling" between topological sectors, the threefold quasidegeneracy remains well-below the continuum states all the way to H_2. These results are qualitatively similar to those using the spherical geometry (Fig. 4) and lend even more support for the adiabatic continuity between Ψ_2 and Ψ_{Pf}. For $N = 10$ and $N = 14$, we did not find a paired ground state on the torus for H_2 with the rectangular unit cell. For these particle numbers the ground state is not threefold degenerate and occurred at wave vectors different from the paired states. This could be due to a finite-size effect which favors non-uniform states on the torus for the H_2 model with the rectangular unit cell [9].

B. Adiabatic continuity in the quasihole sector: Non-Abelian anyons in a particle-hole-symmetric model

The quasihole sector of H_3 supports non-Abelian excitations that can be utilized as building blocks for a topological
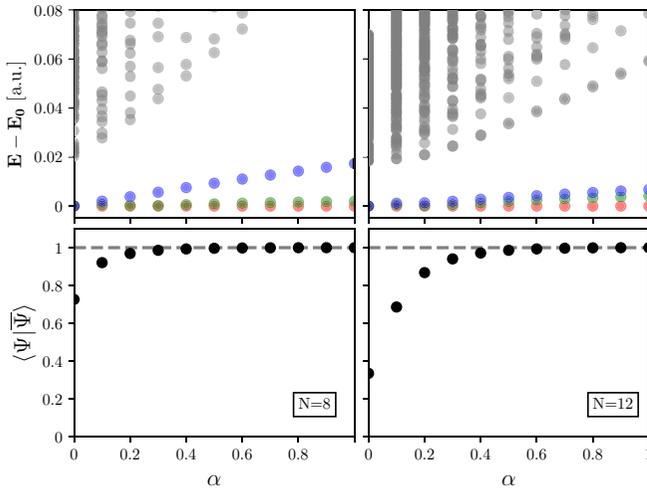
FIG. 6. Relative energy of $H(\alpha)$ in the torus geometry for $N = 8$ (upper-left panel) and $N = 12$ (upper-right panel) for an aspect ratio $\tau = 0.95$ as a function of α. The threefold ground-state degeneracy remains quasidegenerate, and well below the gap, as α is tuned from H_3 to H_2. The bottom panels show the corresponding overlap $\langle \Psi | \overline{\Psi} \rangle$, indicating that Ψ_2 is PH-symmetric at $\alpha = 1$ since $\langle \Psi_2 | \overline{\Psi_2} \rangle = 1$, Ψ_{Pf} breaks PH-symmetry since $\langle \Psi_{\mathrm{Pf}} | \overline{\Psi_{\mathrm{Pf}}} \rangle \neq 1$, and Ψ, the ground state of $H(\alpha)$, remains largely PH-symmetric for finite α less than unity.

quantum computer [34]. To search for the same feature in H_2 we study the quasiholes in the spherical geometry where $2Q = 2N - 2$ is a system with two non-Abelian quasihole excitations. In this geometry, the non-Abelian nature of the excitations manifests through the existence of a zero-energy manifold of states [36]. For topological quantum computing applications it is important that the non-Abelian excitations be degenerate, or at least, the quasidegenerate states must be significantly below the energy gap to generic excitations such that at low temperatures and weak disorder there is an exponentially suppressed probability of the system exciting generic excitations.

In Fig. 7 for $\alpha = 0$ the degenerate manifold of zero-energy states of H_3 is clearly visible. When $\alpha \neq 0$ the degeneracy of the zero-energy manifold is broken by adding any amount of H_2. However, even as $\alpha \to 1$ the spread of the quasidegenerate manifold stays well below the gap to generic excitations. Hence, even the exactly degenerate non-Abelian quasihole states of H_3 are adiabatically connected to the quasidegenerate non-Abelian quasihole states of H_2 for finite-sized systems ($N = 8, 10, 12$ show similar behavior). Again, as we did when studying the ground-state sector, we investigate the thermodynamic limit of this apparent adiabatic continuity of the two quasihole sector.

While it is true that the quasidegenerate manifold of quasihole states remains below the continuum for all system sizes investigated and adiabatic continuity appears manifest, we do observe the degeneracy of the quasihole states of H_3 to be broken upon the inclusion of the two-body term of H_2. Also, the spread in energy of the quasidegenerate states monotonically increases with α. To investigate this in more detail we define δ to be the average energy of the quasidegenerate quasihole
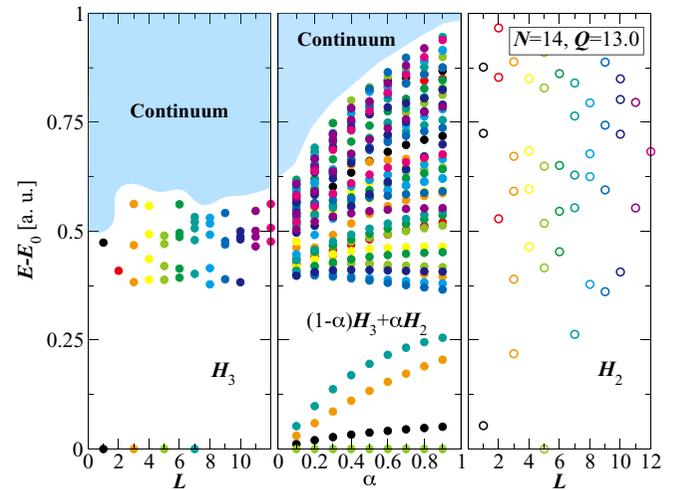

FIG. 7. Energy of $H(\alpha)$ relative to the ground state (see Fig. 4) for the system containing two quasihole excitations ($N = 14$ and $Q = 13$) (the blue sections on the left and middle panels indicate there are higher energy states in the continuum we did not calculate). Nonzero α causes the zero-energy degenerate non-Abelian quasihole manifold to be broken; however, the spread of states stays below the continuum of generic excitations all the way to $\alpha = 1$.

manifold of $H(\alpha)$ and Δ to be the gap between the lowest energy state in the continuum and δ.

As we tune α close to H_2 (Fig. 8), the thermodynamic limit of δ (δ_{therm}) saturates to a value well below the thermodynamic limit of the neutral gap. But Δ_{therm} (the thermodynamic limit of Δ), by contrast, is reduced with increasing α. Moreover, δ_{therm} becomes larger than Δ_{therm} for $\alpha \gtrsim 0.6$–0.8, indicating for infinite system sizes the gap between the ground state and low-lying excited states closes for two-body interactions. Naively this would mean the low-energy states of H_3 and
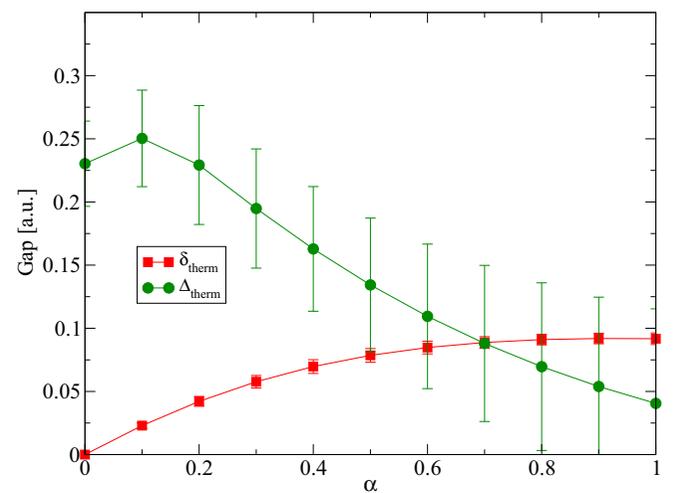

FIG. 8. The thermodynamic limit of the quasihole average energy, δ_{therm} (red), and the energy gap to the generic continuum of states, Δ_{therm} (green), as a function of α. At $\alpha \sim 0.7$ the spread of the quasidegenerate quasiholes bleeds into the continuum and appears to indicate the adiabatic continuity between the low-energy states in the quasihole sector of H_2 and H_3 is lost.

H_2 for two quasiholes are not adiabatically connected. It appears the loss of adiabatic continuity between H_3 and H_2 in the quasihole sector is at odds with the ground-state sector which shows clear and robust adiabatic continuity. Or, perhaps, purely two-body interactions cannot host non-Abelian quasihole excitations. But, as we argue below, the transition to $\delta_{\text{therm}}/\Delta_{\text{therm}} > 1$ is due to a finite-size effect limitation of our exact calculations.

The breaking of the degeneracy of the non-Abelian quasiholes can be impacted by at least two causes. First, the low-energy states are simply not adiabatically connected. However, Fig. 7, while showing a spreading of the quasidegenerate states with α, clearly shows the same states staying below the continuum. Appendix B also shows a detailed tracking of individual states and, again, the states are adiabatically connected and never mix or cross higher-energy generic states in the continuum. The quasidegenerate states of $H(\alpha)$ also maintain high overlaps with the exactly degenerate quasihole states of H_3 (see Appendix B).

The second possible cause of the broken degeneracy in the quasihole manifold stems from a finite-size effect. The quasiholes themselves are finite and can overlap in real space. The addition of the two-body interaction term in H_2 produces an energy cost for this overlap in quasiholes, breaking the degeneracy [34]. In that case, the quasidegenerate states with the smallest total L would be the least affected because they correspond to the states with the quasiholes the furthest away from one another [6,56]. To test for this effect we compute the energy gap (Δ_{therm}^1) between the lowest energy in the continuum and the energy of the quasihole state with the smallest L (not necessarily the smallest energy), i.e., $L = 0$, 1, 0, and 1 for $N = 8$, 10, 12, and 14, respectively, in the thermodynamic limit. Fig. 9 shows this gap is well-defined (note the smaller error bars in the linear extrapolation) and finite in the thermodynamic limit and the smallest L state of the quasidegenerate quasihole states of H_3 and H_2 remain adiabatically connected. Our results indicate the size and physical overlap of quasiholes (for large L) likely is leading to a finite-size effect that undermines adiabaticity in our finite-size study of the quasihole gap.

To further elucidate the above, we study the gap between the lowest energy state in the continuum and the lowest *energy* state of the quasidegenerate manifold of quasihole states (Δ_{therm}^2 [not shown]), i.e., $L = 2$, 3, 4, and 5 for $N = 8$, 10, 12, and 14, respectively. In contrast to Δ_{therm}^1, Δ_{therm}^2 is not well-behaved and eventually decreases and bleeds into δ_{therm}. The error of this extrapolation is also very large indicating the extrapolation is not particularly linear. This behavior is consistent with the explanation that the degeneracy is broken due to interactions between the quasiholes in a finite-sized system caused by the two-body interaction of H_2.

The four-quasihole sector at $2Q = 2N - 1$ does not show reasonable adiabatic continuity as the degenerate manifold is broken badly by H_2 and bleeds into the continuum at finite $\alpha \lesssim 0.5$ [57]. From the above discussion of quasiparticle size we conclude that the apparent lack of adiabatic continuity is a reflection of quasihole interactions between closely spaced quasiholes in our finite-sized system studies. We do find, however, that well-separated quasiholes retain adiabatic continuity in the thermodynamic limit.
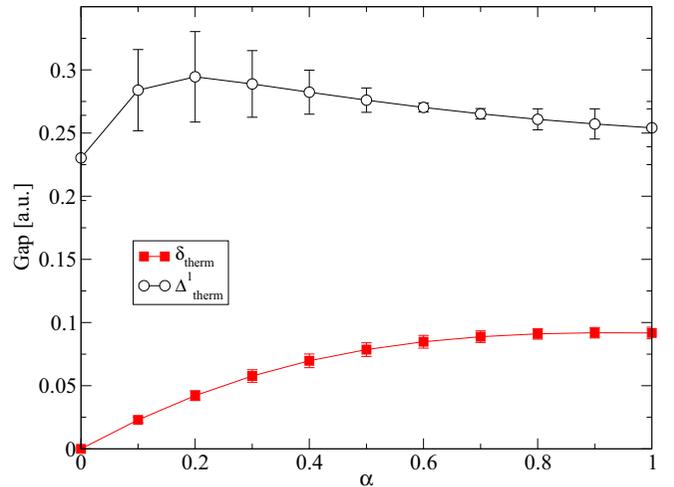

FIG. 9. The thermodynamic limit of the gaps between the lowest energy state in the continuum and the smallest angular momentum states of the quasidegenerate manifold Δ_{therm}^1, i.e., $L = 0, 1, 0$, and 1 for $N = 8, 10, 12$, and 14, respectively. This gap (black open circles) is well behaved and linear in $1/N$ as indicated by the small error bars in the extrapolation. Finite-size effects have been greatly reduced in comparison to Fig. 8 and the spread in the (quasi)degenerate quasihole energy remains below the gap to generic states in the continuum.

V. PARTICLE-HOLE-SYMMETRY

Physical two-body interactions are PH symmetric and so we expect ground states of two-body Hamiltonians at half-filling to also be PH symmetric in the absence of spontaneous PH symmetry breaking. In this section we show that, for finite systems sizes on the torus, Ψ_2 remains robustly PH symmetric even under PH-symmetry breaking perturbations. Moreover, we argue that prior evidence for spontaneously broken PH symmetry on the sphere [44] can be interpreted as a expression of an even-odd effect. We conclude that our numerical calculations do not show unambiguous evidence that H_2 spontaneously breaks PH symmetry.

We begin by noting that Ψ_2 is nearly identical to the Moore-Read Pfaffian. (Note the PH conjugate of Ψ_2 compares equally well to the anti-Pfaffian since H_2 is PH symmetric.) The numerical wave function overlaps for various system sizes given in Table I quantify how "identical" Ψ_2 is compared to Ψ_{Pf}. The overlap is above 0.96 for systems up to $N = 16$. The proximity of these overlaps to unity compares to overlaps found between CF wave functions for odd-denominator FQH states of the form $\nu = n_0/(2pn_0 \pm 1)$ and the pure Coulomb ground state in the LLL [6].

TABLE I. Numerical wave function overlaps between Ψ_2 and Ψ_{Pf} on the sphere. Note the overlaps between Ψ_2 at the Moore-Read anti-Pfaffian shift $2Q = 2N + 1$ and the Moore-Read anti-Pfaffian state Ψ_{aPf} are identical to those listed below for $N \to N - 2$.

N	8	10	12	14	16
$\langle \Psi_2 \| \Psi_{\text{Pf}} \rangle$	0.9997	0.9951	0.9869	0.9724	0.96345

In the past, it was found that PH symmetrization (on the torus) was able to increase the overlap of Ψ_{Pf} with the ground state of the Coulomb interaction for $\nu = 5/2$ [9]. Thus, perhaps Ψ_2 is identical (or very close) to the PH symmetrized Ψ_{Pf}. After all, Ψ_2 is the ground state of $H_2 = H_3 + \overline{H}_3$, with each term producing Ψ_{Pf} and Ψ_{aPf} independently. For $N = 12$ on the torus the overlap between the PH symmetrized Ψ_{Pf} and Ψ_2 is 0.849 while the overlaps between Ψ_2 and Ψ_{Pf} and Ψ_{aPf} are both 0.694 (see Appendix C). So the PH symmetrized Ψ_{Pf} is not identical to Ψ_2 and we conclude that simple operations acting on Ψ_{Pf} (and/or Ψ_{aPf}) do not generate Ψ_2 with high accuracy.

We now consider the possibility of spontaneous PH symmetry breaking of Ψ_2 [44]. If Ψ_{Pf} explicitly breaks PH symmetry, and the overlap between Ψ_2 and Ψ_{Pf} is so close to unity, then perhaps Ψ_2 spontaneously breaks PH symmetry. In fact, it has been argued [45,46] that a ground-state adiabatically connected to Ψ_{Pf} must break PH symmetry spontaneously. Reference [44] worked exclusively in the spherical geometry and checking whether $\langle \Psi | \overline{\Psi} \rangle$ is unity, to determine PH symmetry, is not straightforward. Instead, the ground-state energy of H_2 was examined as a function of N (for various flux $2Q$) in the vicinity of half-filling. The ground-state energy of H_2 was found to be lower for situations when $2Q = 2N - 3$ or $2Q = 2N + 1$ for N even exhibiting a "wine-bottle" structure. This was interpreted as evidence for spontaneous PH symmetry breaking.

However, it is possible the "wine-bottle" structure instead points to an even-odd effect. In Ref. [47], the ground-state energy per particle of H_2 was calculated for $2Q = 2N - 3$ from $N = 4$ to 18 and showed a distinct even-odd effect. The even-odd effect is consistent with a paired ground state (recall, it has high overlap with the paired Moore-Read Pfaffian state). The even-odd effect in the finite-size calculations could have been the underlying cause of the "wine-bottle"-shaped energy profile. Thus, it is unclear if Ψ_2 actually spontaneously breaks PH symmetry or is simply a paired state exhibiting an even-odd effect (or both). As mentioned above, it is difficult in the spherical geometry to check PH symmetry through the calculation of $\langle \Psi | \overline{\Psi} \rangle$ due to the spherical shift S. The shift, in a sense, explicitly breaks PH symmetry in the basis states themselves (except for the case $S = 0$ at $2Q = 2N - 1$). As a result of the shift, taking the PH conjugate of Ψ_2 or Ψ_{Pf} at $2Q = 2N - 3$ changes N at constant flux or changes the flux at constant N. This complicates the analysis [58]. In contrast, it is straightforward to compute $\langle \Psi | \overline{\Psi} \rangle$ on the torus since the shift is zero and the PH conjugate of Ψ has the same quantum numbers as Ψ. If Ψ is PH-symmetric, then $\langle \Psi | \overline{\Psi} \rangle = 1$.

The lower two panels of Fig. 6 show $\langle \Psi | \overline{\Psi} \rangle$ for $H(\alpha)$ and $N = 8$ and $N = 12$. The data at $H(0) = H_3$ show clearly that Ψ_{Pf} breaks PH symmetry, as expected, and at $H(1) = H_2$, Ψ_2 is PH symmetric, as expected for the ground state of a two-body Hamiltonian. Interestingly, for the larger system size ($N = 12$) three additional states appear to be separating from the continuum. Reference [46] pointed out that the degeneracy in the thermodynamic limit of a PH symmetric state in the Pfaffian universality class would theoretically carry a sixfold degeneracy with the extra factor of two arising from PH symmetry (we have already subsumed a factor of two due to center-of-mass). Our calculation is seemingly the first

indication of this effect that is typically absent due to strong finite-size effects. Importantly, Ψ_2 remains PH-symmetric even with the explicit PH symmetry breaking term $(1 - \alpha)H_3$ added. We find that as α is reduced from unity, the additional term does not immediately break PH symmetry and the ground state Ψ of $H(\alpha)$ remains robustly PH symmetric for finite values of α. If the ground state were to spontaneously break PH-symmetry, we would expect $\langle \Psi | \overline{\Psi} \rangle$ to behave qualitatively different as a function of α [37].

Before ending this section we briefly consider the ground-state energy of H_2 at the PH symmetric shift ($S = -1$) in the spherical geometry ($2Q = 2N - 1$) and ask whether the ground state might be related to the so-called PH-Pfaffian state [59–63]. The PH-Pfaffian has been discussed in relation to recent puzzling experimental results regarding the thermal Hall conductivity at $\nu = 5/2$ [64]. Reference [65] inadvertently computed the ground state of H_2 in the spherical geometry. Figure 3 and Appendix A of that work studied all even N from $N = 8$ to 16. A uniform ground state with $L = 0$ was *only* found for $N = 12$ for H_2—all other systems were compressible. These results indicate the ground state of H_2 is not consistent with the PH-Pfaffian.

To summarize this section, the bottom panels in Fig. 6 suggest that H_2 does *not* spontaneously break PH symmetry. This surprising result leads us back to the "wine-bottle" result of Ref. [44]. One interpretation of Ref. [44] is that the "wine-bottle" merely reflects electron pairing without PH symmetry breaking. Another possibility is that results presented in Fig. 6 are far from the thermodynamic limit and cannot capture spontaneous PH symmetry breaking. We therefore conclude the finite-size results have so far not settled the issue of whether or not H_2 spontaneously breaks PH symmetry.

VI. ENTANGLEMENT PROPERTIES

To further study the topological order of Ψ_2 we examine its quantum entanglement properties. Here we definitively show that Ψ_2 is in the same universality class as the Moore-Read Pfaffian/anti-Pfaffian by investigating the topological entanglement entropy and spectrum.

A. Topological entanglement entropy

The topological entanglement entropy of a wave function Ψ is found by dividing the system into two pieces (A and B) and calculating the von Neumann entropy S_A of the partial density matrix of region A by tracing out all degrees of freedom in B of the total density matrix. This entropy measures the degree to which the wave function's degrees of freedom in the two subsystems are entangled [66]. A state's topological order manifests as a reduction in S_A [67,68] as

$$S_A = a L_S - \gamma_\Psi + \mathcal{O}(1/L_S), \quad (5)$$

where a is a nonuniversal constant, L_S is the length of the boundary between the two subsystems, and $\gamma_\Psi > 0$ is the topological entanglement entropy.

We will utilize the spherical geometry for this calculation and consider an orbital partition: geometrically we are partitioning the sphere along a lines of latitude. The aim is to determine γ_{Ψ_2} for Ψ_2 compared with the topological

TABLE II. Entanglement entropy S_{l_A} as a function of l_A for Ψ_2 for $N = 6, 8, 10, 12,$ and 14. These numbers should be compared to those of the Moore-Read Pfaffian given in Ref. [69].

l_A	$N = 6$	8	10	12	14
1	0.67301	0.68291	0.68696	0.68901	0.69019
2	1.15777	1.23414	1.24039	1.24491	1.25173
3	1.49971	1.65389	1.68975	1.71084	1.72946
4	1.76712	2.03339	2.09498	2.13745	2.17107
5	**1.88152**	2.31556	2.43072	2.50253	2.55808
6		2.48129	2.68508	2.80127	2.88807
7		**2.54204**	2.86597	3.04219	3.16802
8			2.97194	3.22674	3.39942
9			**3.00718**	3.35726	3.58560
10				3.4354	3.72965
11				**3.4609**	3.83228
12					3.89415
13					**3.91462**

entanglement entropy of the Moore-Read Pfaffian, known exactly to be $\gamma_{\Psi_{Pf}} = \ln\sqrt{8}$ [13,69]. For a topologically ordered state, $\gamma_\Psi = \ln\mathcal{D}$ where $\mathcal{D} = \sqrt{\sum d_i^2}$ is the total quantum dimension and d_i are the quantum dimensions of the quasiparticles excitations of the theory [34].

We follow Zozulya *et al.* [69] in our calculation of γ_{Ψ_2} and calculate S_A for various lengths L_S to find the "y intercept" γ_Ψ. We focus on systems for which $2Q = 2N - 3$ and partition along a z-component of angular momentum l_A. This orbital partition corresponds to partition at a LLL single-particle state of the form $\eta_{l_A}(z) \sim z^{l_A}\exp(-|z|^2/4)$ as the spherical radius is taken to infinity. The radius of this state is proportional to $\sqrt{l_A}$ so the boundary length $L_S \propto \sqrt{l_A}$. A partition of the sphere along an orbital corresponding to l_A gives an expected entanglement entropy of the form $S_A = a\sqrt{l_A} - \gamma_\Psi + \mathcal{O}(1/\sqrt{l_A})$. However, the fact that we must calculate for a finite sphere and take the thermodynamic limit makes this procedure more involved. In fact, the entanglement entropy of $S_B = S_A$ so, for a given N (and therefore Q), we calculate S_A for $l_A = 1, \ldots, (2Q+1)/2$ ($l_A = (2Q+1)/2$ is the equator). Again, following Ref. [69] we label S_A for various partitions l_A as S_{l_A} and Table II gives $S_{l_A}(N)$ as a function of $l_A = 1, \ldots, (2Q+1)/2$ and $N = 6, 8, 10, 12,$ and 14 for Ψ_2. One can compare these values to those calculated for the Moore-Read Pfaffian given in Ref. [69]. Indeed, the entanglement entropy of Ψ_2 is nearly identical to Ψ_{Pf}.

To extrapolate to the thermodynamic limit we construct a linear fit of $S_{l_A}(N)$ versus $1/N$ and the thermodynamic limit ($1/N \to 0$) is determined (see the left panel of Fig. 10). Upper and lower bounds of this extrapolation are used to assign an uncertainty of $\pm|S_{l_A}(0) - S_1|$ where $S_1 = S_{l_A}(x_1)(1 - x_1/(x_1 - x_0) + S_{l_A}(x_0)(x_1/(x_1 - x_0))$ where the two smallest values of N are x_0 and x_1, respectively [69].

A least squares fit of $S_{l_A}(0)$ as a function of $\sqrt{l_A}$ gives $\gamma_{\Psi_2} = 1.27$. To determine the error bars we construct a straight line through the value of $S_{l_A}(0)$ for the largest (smallest) value of l_A plus (minus) $|S_{l_A}(0) - S_1|$ and vice versa. We then determine the negative of the y intercept and an upper and lower bound on γ_{Ψ_2}—these lines are the bounds of the shaded
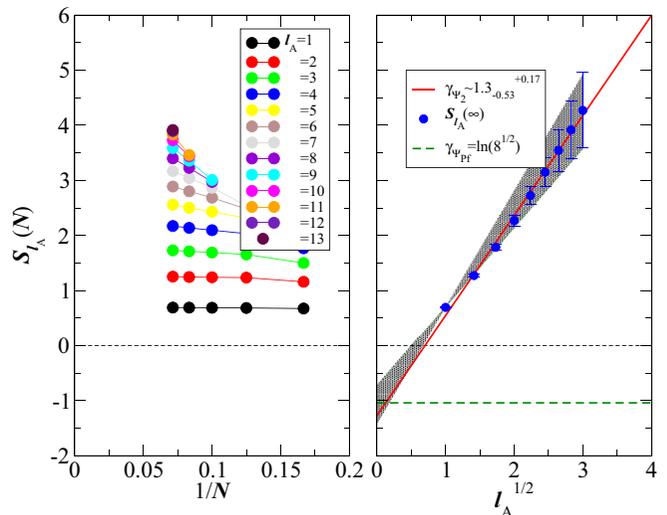

FIG. 10. Entanglement entropy $S_{l_A}(N)$ versus $1/N$ for various l_A for Ψ_2 at $2Q = 2N - 3$ (left panel). The right panel shows the thermodynamic limit $S_{l_A}(\infty)$ versus $\sqrt{l_A}$ to determine the topological entanglement entropy γ_{Ψ_2}. The error bars are uncertainty of the extrapolation (explained in the text) and the shaded region depicts the upper and lower bounds of the extrapolation.

region in the right panel of Fig. 10 finally yielding $\gamma_{\Psi_2} = 1.27^{+0.17}_{-0.53}$. This result contains $\gamma_{Pf} = \ln\sqrt{8} \approx 1.04$ within its error bars. Of course, more work can reduce the error bars in $\gamma_{\Psi_{Pf}}$ as was done for $\gamma_{\Psi_{Pf}}$ in Ref. [69]. Nonetheless, our results show that γ_{Ψ_2} is consistent with $\gamma_{\Psi_{Pf}}$.

B. Topological entanglement spectrum

The entanglement entropy provides limited information about the topological order of a wave function. Consequently, Li and Haldane proposed investigating the entire spectrum of eigenvalues $\{\xi_i\}$ of the reduced density matrix [70].

Figure 11 shows the orbital entanglement spectrum of Ψ_2 and Ψ_{Pf} (with which to compare) for $N = 14$ particles—we note that smaller system sizes show similar results. We report the spectra while partitioning the sphere at the equator (in the notation of Li and Haldane [70] this corresponds to $P[0|0]$ for $N/2$ even and $P[1|1]$ for $N/2$ odd).

The low-lying states of the orbital entanglement spectrum can be used as a "fingerprint" with which to identify topologically ordered states as they are related to the underlying conformal field theory (CFT) of the corresponding FQH state [70–72]. The low-lying states of Ψ_2 very closely match those of Ψ_{Pf} both quantitatively and qualitatively (counting of levels). There is a clear "topological entanglement gap" [70] separating the CFT-like low lying states from the higher "energy" generic non-CFT-like levels.

While the low-lying levels of the entanglement spectrum of Ψ_2 match very closely to those of the Moore-Read Pfaffian (or anti-Pfaffian at the anti-Pfaffian shift), the spectrum of Ψ_2 has many generic non-CFT-like levels similar, qualitatively, to the second LL Coulomb interaction [70,73,74]. From both the entanglement entropy and spectrum it appears that Ψ_2 is in the same universality class as the Moore-Read Pfaffian/anti-Pfaffian.
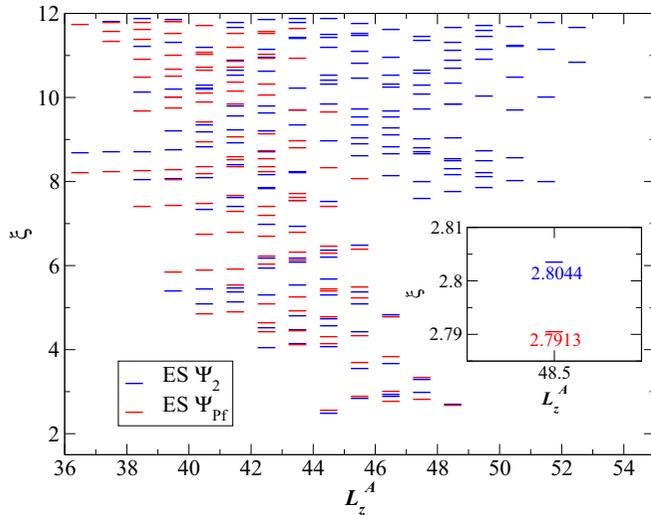
FIG. 11. Orbital entanglement spectrum for Ψ_2 and Moore-Read Pfaffian for $N = 14$. The inset shows the ES of the "root" configuration [70] of both states. The inset shows a zoom in where the states are barely distinguishable. The partition is along the spherical equator, i.e., $P[1|1]$ in the notation of Ref. [70].

VII. SUMMARY

We have studied a physically realistic model for the FQHE in a half-filled LL to investigate to what extent PH symmetry breaking and/or the existence of a generating Hamiltonian with three-body terms, crucial to the realization of exotic states that support non-Abelian anyonic excitations in the universality class of the Moore-Read Pfaffian/anti-Pfaffian?

The model we studied, H_2, is short-ranged and two-body but nonetheless hosts non-Abelian quasihole excitations. We find the two-body model has roton and neutral fermion modes as well as quasiparticle pairing as indicated by an even-odd effect and strong overlap with the Moore-Read Pfaffian/anti-Pfaffian. Furthermore, we find, via entanglement measures, the ground state Ψ_2 is in the universality class of the Moore-Read Pfaffian/anti-Pfaffian.

Our most important finding is that the low-energy excitations of the Moore-Read Pfaffian are adiabatically connected to those of the physically realistic two-body model H_2. These excitations include non-Abelian anyons. Ideally, anyons reside in a topologically protected exactly degenerate manifold. We find, however, a small splitting between these degenerate states likely persists even in the thermodynamic limit, hence, it is possible the splitting is caused by "tunneling" between sectors defined by the PH symmetrization operator. While this splitting remains below all energy gaps, further exploration of the cause of this splitting will be useful in establishing the robustness of topological protection in topological quantum computing proposals.

H_2 is a physically realistic model which therefore lends itself to quantum state engineering. For example, efforts to realize the LLL with ultracold atoms [75–78] are more likely to be able to engineer H_2 than H_3. Further work to realize H_2 with ultracold fermions (or Bosonic counterpart models with ultracold bosons) could lead to the exciting possibility of non-Abelian anyons in a tunable environment.

APPENDIX A: HALDANE PSEUDOPOTENTIAL EXPANSION OF H_2 ON THE SPHERE FOR FINITE SYSTEM SIZES

Any two-body interaction Hamiltonian can be characterized in terms of Haldane pseudopotentials V_m. The only nonzero Haldane pseudopotenials for H_2 are V_1 and V_3 [44]. To see this we write $H_3 + \overline{H}_3$ and, after cancellation of the three-body terms, construct the remaining finite-size two-body terms on the sphere:

$$H_2 = V_1^{2Q} \sum_{i<j} \hat{P}_{ij}(1) + V_3^{2Q} \sum_{i<j} \hat{P}_{ij}(3), \qquad (A1)$$

with all other $V_m^{2Q} = 0$ for all even m and for all odd $m > 3$ (here, m is the pair relative angular momentum in the planar geometry after the appropriate stereographic mapping [79]). Table III and Fig. 12 give the values of V_1 and V_3, and their ratio V_1/V_3, for some relevant system sizes. Additionally, one can extrapolate the finite-sized spherical pseudopotentials to the thermodynamic limit yielding the pseudopotentials in the planar geometry. The ratio V_1/V_3 equals three to high precision in the thermodynamic limit. We note that in Ref. [44] the pseudopotential values in the thermodynamic limit were given incorrectly, however, all ratios were correct and all results therein remain unchanged.

TABLE III. In the thermodynamic limit $V_1 = 3.37496(9)$, $V_3 = 1.12368(15)$, and $V_1/V_3 = 3.00074(8)$. To a high degree of accuracy, one can calculate V_1^{2Q} and V_3^{2Q} at values of Q in between those given in the table through interpolation—however, you could contact the corresponding author who will be happy to give you values up to around $2Q = 32$.

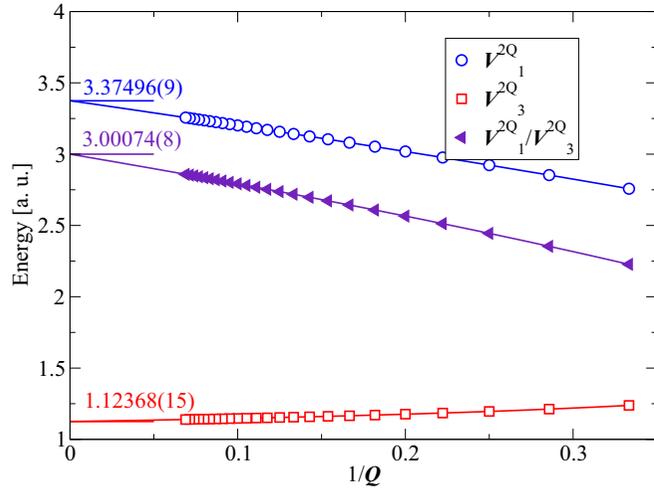| $2Q$	V_1^{2Q}	V_3^{2Q}	V_1^{2Q}/V_3^{2Q}
9	2.976470	1.184615	2.512605
13	3.104367	1.161498	2.672727
17	3.170137	1.151297	2.753535
21	3.210124	1.145527	2.802312
25	3.237082	1.141844	2.834960
29	3.256420	1.139266	2.858349
31	3.264240	1.138269	2.867722

FIG. 12. The finite-sized Haldane pseudopotentials V_1^{2Q}, V_3^{2Q}, and the ratio V_1^{2Q}/V_3^{2Q} of H_2 are shown versus the inverse system size ($1/Q$). The values of V_1, V_3, and V_1/V_3 in the thermodynamic limit ($1/Q \to 0$) are shown on the y axis and found via a fourth-order polynomial extrapolation. The value $V_1/V_3 \to 3$ is used in the first line of Eq. (2).

Finally, the planar values $V_1 = 3.375$ and $V_3 = 1.125$ were found in a very different calculation recently [80] as the "leading-order" terms in a type of mean-field two-body approximation of a generic three-body interaction term.

APPENDIX B: TRACKING STATES

In Fig. 13 we track individual low-energy states of $H(\alpha)$ more precisely. The figure shows the lowest 50 states as a function of their "index" for $N = 8$, 10, 12, and 14 for $\alpha = 0$, 0.5, and 1. The quasidegenerate states remain inside the gap and adiabatic quasidegeneracy is maintained. More evidence for adiabaticity can be found by calculating the wave function overlap between the quasidegenerate states of $H(\alpha)$ and the
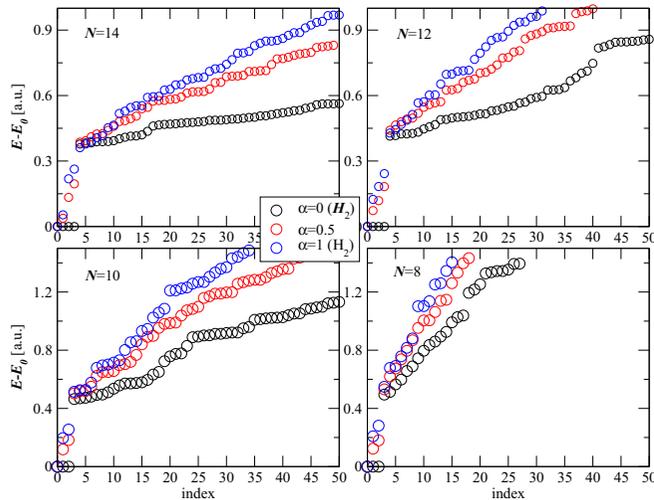

FIG. 13. The lowest 50 states as of $H(\alpha)$ a function of "index" for $N = 8$, 10, 12, and 14 for $\alpha = 0$, 0.5, and 1.
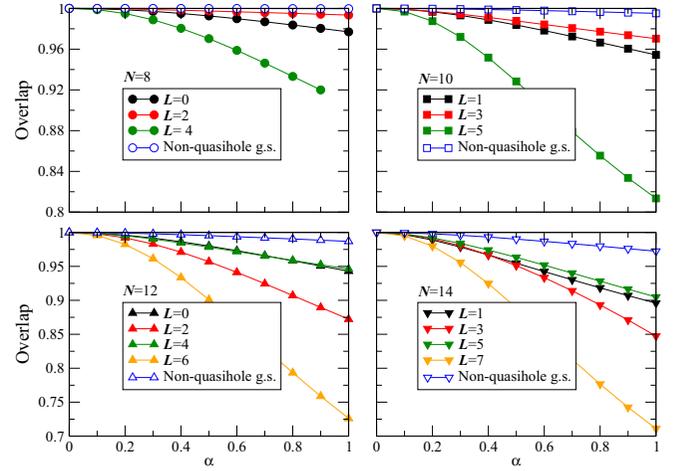

FIG. 14. The wave function overlap of the exactly degenerate quasihole states, labeled by their angular momentum L, of H_3 with the quasidegenerate quasihole states of $H(\alpha)$ as a function of α for $N = 8$, 10, 12, and 14. Additionally, the open symbols are the overlaps between the Moore-Read Pfaffian and the ground state of $H(\alpha)$ for the ground-state sector. All overlaps are trivially one for $\alpha = 0$ and remain large (typically above 0.9 for states with small angular momentum L).

exactly degenerate states of H_3. In Fig. 14 we see the overlaps remain extremely high for each state in the quasidegeneracy.

APPENDIX C: COMBINING MOORE-READ PFAFFIAN AND ANTI-PFAFFIAN STATES

We can combine the Moore-Read Pfaffian and anti-Pfaffian states to attempt a variational ground state that captures the properties of Ψ_2. We work on the torus to combine these states in an explicit method that effectively PH symmetrizes Ψ_{Pf}. We first note that $\langle \Psi_{Pf} | \Psi_{aPf} \rangle \neq 0$ on the torus. Therefore, we use a variant of the Gram-Schmidt procedure (Löwdin symmetric orthogonalization) to combine the states. The transformation is

$$|\Psi'_{Pf}\rangle = c_+ |\Psi_{Pf}\rangle + c_- |\Psi_{aPf}\rangle, \qquad (C1)$$

$$|\Psi'_{aPf}\rangle = c_- |\Psi_{Pf}\rangle + c_+ |\Psi_{aPf}\rangle, \qquad (C2)$$

where

$$c_\pm = \frac{1}{2}\left(\frac{1}{\sqrt{1 \mp \langle \Psi_{Pf} | \Psi_{aPf} \rangle}} \pm \frac{1}{\sqrt{1 \pm \langle \Psi_{Pf} | \Psi_{aPf} \rangle}} \right). \quad (C3)$$

Now we see that each state is orthonormal, $\langle \Psi'_{Pf} | \Psi'_{aPf} \rangle = 0$, and the two states are PH conjugates of each other. Using the above orthogonal states we can construct a PH symmetric state:

$$|\Psi\rangle = \frac{|\Psi'_{Pf}\rangle + |\Psi'_{aPf}\rangle}{\sqrt{2}}. \qquad (C4)$$

For $N = 12$ (aspect ratio $\tau = 0.95$) the original overlaps are $\langle \Psi_2 | \Psi_{Pf} \rangle = 0.693542 = \langle \Psi_2 | \Psi_{aPf} \rangle$ and $\langle \Psi_{Pf} | \Psi_{aPf} \rangle = 0.336155$. Finally, we find that $\langle \Psi_2 | \Psi \rangle = 0.848514$. Evidently, Ψ_2 not identical to a linear combination of Ψ_{Pf} and its PH conjugate.

[1] R. B. Laughlin, Phys. Rev. Lett. **50**, 1395 (1983).

[2] D. C. Tsui, H. L. Stormer, and A. C. Gossard, Phys. Rev. Lett. **48**, 1559 (1982).

[3] F. D. M. Haldane, Phys. Rev. Lett. **51**, 605 (1983).

[4] S. A. Trugman and S. Kivelson, Phys. Rev. B **31**, 5280 (1985).

[5] J. K. Jain, Phys. Rev. Lett. **63**, 199 (1989).

[6] J. Jain, *Composite Fermions* (Cambridge University Press, Cambridge, 2007).

[7] B. I. Halperin, P. A. Lee, and N. Read, Phys. Rev. B **47**, 7312 (1993).

[8] E. Rezayi and N. Read, Phys. Rev. Lett. **72**, 900 (1994).

[9] E. H. Rezayi and F. D. M. Haldane, Phys. Rev. Lett. **84**, 4685 (2000).

[10] S. D. Geraedts, M. P. Zaletel, R. S. K. Mong, M. A. Metlitski, A. Vishwanath, and O. I. Motrunich, Science **352**, 197 (2016).

[11] R. L. Willett, R. R. Ruel, K. W. West, and L. N. Pfeiffer, Phys. Rev. Lett. **71**, 3846 (1993).

[12] R. Willett, J. P. Eisenstein, H. L. Stormer, D. C. Tsui, A. C. Gossard, and J. H. English, Phys. Rev. Lett. **59**, 1776 (1987).

[13] G. Moore and N. Read, Nucl. Phys. B **360**, 362 (1991).

[14] V. W. Scarola, K. Park, and J. K. Jain, Nature **406**, 863 (2000).

[15] G. Möller and S. H. Simon, Phys. Rev. B **77**, 075319 (2008).

[16] N. Read and D. Green, Phys. Rev. B **61**, 10267 (2000).

[17] R. H. Morf, Phys. Rev. Lett. **80**, 1505 (1998).

[18] M. R. Peterson, T. Jolicoeur, and S. Das Sarma, Phys. Rev. Lett. **101**, 016807 (2008).

[19] M. R. Peterson, T. Jolicoeur, and S. Das Sarma, Phys. Rev. B **78**, 155308 (2008).

[20] A. E. Feiguin, E. Rezayi, C. Nayak, and S. Das Sarma, Phys. Rev. Lett. **100**, 166803 (2008).

[21] A. E. Feiguin, E. Rezayi, K. Yang, C. Nayak, and S. Das Sarma, Phys. Rev. B **79**, 115322 (2009).

[22] A. Wójs, C. Tőke, and J. K. Jain, Phys. Rev. Lett. **105**, 096802 (2010).

[23] M. Storni, R. H. Morf, and S. Das Sarma, Phys. Rev. Lett. **104**, 076803 (2010).

[24] E. H. Rezayi and S. H. Simon, Phys. Rev. Lett. **106**, 116801 (2011).

[25] K. Pakrouski, M. R. Peterson, T. Jolicoeur, V. W. Scarola, C. Nayak, and M. Troyer, Phys. Rev. X **5**, 021004 (2015).

[26] M. P. Zaletel, R. S. K. Mong, F. Pollmann, and E. H. Rezayi, Phys. Rev. B **91**, 045115 (2015).

[27] A. Tylan-Tyler and Y. Lyanda-Geller, Phys. Rev. B **91**, 205404 (2015).

[28] E. H. Rezayi, Phys. Rev. Lett. **119**, 026801 (2017).

[29] C. Nayak and F. Wilczek, Nucl. Phys. B **479**, 529 (1996).

[30] Y. Tserkovnyak and S. H. Simon, Phys. Rev. Lett. **90**, 016802 (2003).

[31] M. Baraban, G. Zikos, N. Bonesteel, and S. H. Simon, Phys. Rev. Lett. **103**, 076801 (2009).

[32] P. Bonderson, V. Gurarie, and C. Nayak, Phys. Rev. B **83**, 075303 (2011).

[33] S. Das Sarma, M. Freedman, and C. Nayak, Phys. Rev. Lett. **94**, 166802 (2005).

[34] C. Nayak, S. H. Simon, A. Stern, M. Freedman, and S. Das Sarma, Rev. Mod. Phys. **80**, 1083 (2008).

[35] M. Greiter, X.-G. Wen, and F. Wilczek, Phys. Rev. Lett. **66**, 3205 (1991).

[36] N. Read and E. Rezayi, Phys. Rev. B **54**, 16864 (1996).

[37] H. Wang, D. N. Sheng, and F. D. M. Haldane, Phys. Rev. B **80**, 241311 (2009).

[38] W. Bishara and C. Nayak, Phys. Rev. B **80**, 121302 (2009).

[39] M. R. Peterson and C. Nayak, Phys. Rev. B **87**, 245129 (2013).

[40] I. Sodemann and A. H. MacDonald, Phys. Rev. B **87**, 245425 (2013).

[41] S. H. Simon and E. H. Rezayi, Phys. Rev. B **87**, 155426 (2013).

[42] R. E. Wooten, J. H. Macek, and J. J. Quinn, Phys. Rev. B **88**, 155421 (2013).

[43] C. Toke and J. K. Jain, Phys. Rev. Lett. **96**, 246805 (2006).

[44] M. R. Peterson, K. Park, and S. Das Sarma, Phys. Rev. Lett. **101**, 156803 (2008).

[45] S.-S. Lee, S. Ryu, C. Nayak, and M. P. A. Fisher, Phys. Rev. Lett. **99**, 236807 (2007).

[46] M. Levin, B. I. Halperin, and B. Rosenow, Phys. Rev. Lett. **99**, 236806 (2007).

[47] H. Lu, S. Das Sarma, and K. Park, Phys. Rev. B **82**, 201303 (2010).

[48] G. Möller, A. Wójs, and N. R. Cooper, Phys. Rev. Lett. **107**, 036803 (2011).

[49] U. Wurstbauer, K. W. West, L. N. Pfeiffer, and A. Pinczuk, Phys. Rev. Lett. **110**, 026801 (2013).

[50] Numerical studies find the ground state of the realistic Coulomb interaction at $\nu = 5/2$ is fully spin-polarized [17,21,81,82]. Experiments, however, are somewhat mixed [83–85].

[51] W. Kohn and J. M. Luttinger, Phys. Rev. Lett. **15**, 524 (1965).

[52] A. V. Chubukov, Phys. Rev. B **48**, 1097 (1993).

[53] X. G. Wen and Q. Niu, Phys. Rev. B **41**, 9377 (1990).

[54] P. Bonderson, A. E. Feiguin, and C. Nayak, Phys. Rev. Lett. **106**, 186802 (2011).

[55] M. Greiter, X. G. Wen, and F. Wilczek, Nucl. Phys. B **374**, 567 (1992).

[56] P. Sitko, S. N. Yi, K. S. Yi, and J. J. Quinn, Phys. Rev. Lett. **76**, 3396 (1996).

[57] W. Hutzel, M.Sc. thesis, California State University Long Beach, 2018.

[58] K. Pakrouski, M. Troyer, Y.-L. Wu, S. Das Sarma, and M. R. Peterson, Phys. Rev. B **94**, 075108 (2016).

[59] D. T. Son, Phys. Rev. X **5**, 031027 (2015).

[60] P. Bonderson, C. Nayak, and X.-L. Qi, J. Stat. Mech.: Theory Exp. (2013) P09016.

[61] X. Chen, L. Fidkowski, and A. Vishwanath, Phys. Rev. B **89**, 165132 (2014).

[62] M. V. Milovanović, M. D. Ćirić, and V. Juričić, Phys. Rev. B **94**, 115304 (2016).

[63] R. V. Mishmash, D. F. Mross, J. Alicea, and O. I. Motrunich, Phys. Rev. B **98**, 081107 (2018).

[64] M. Banerjee, M. Heiblum, V. Umansky, D. E. Feldman, Y. Oreg, and A. Stern, Nature **559**, 205 (2018).

[65] A. C. Balram, M. Barkeshli, and M. S. Rudner, Phys. Rev. B **98**, 035127 (2018).

[66] M. Srednicki, Phys. Rev. Lett. **71**, 666 (1993).

[67] A. Y. Kitaev and J. Preskill, Phys. Rev. Lett. **96**, 110404 (2006).

[68] M. A. Levin and X.-G. Wen, Phys. Rev. Lett. **96**, 110405 (2006).

[69] O. S. Zozulya, M. Haque, K. Schoutens, and E. H. Rezayi, Phys. Rev. B **76**, 125310 (2007).

[70] H. Li and F. D. M. Haldane, Phys. Rev. Lett. **101**, 010504 (2008).

[71] A. Chandran, M. Hermanns, N. Regnault, and B. A. Bernevig, Phys. Rev. B **84**, 205136 (2011).

[72] X.-L. Qi, H. Katsura, and A. W. W. Ludwig, Phys. Rev. Lett. **108**, 196402 (2012).

[73] J. Zhao, D. N. Sheng, and F. D. M. Haldane, Phys. Rev. B **83**, 195135 (2011).

[74] J. Biddle, M. R. Peterson, and S. Das Sarma, Phys. Rev. B **84**, 125141 (2011).

[75] M. Lewenstein, A. Sanpera, V. Ahufinger, B. Damski, A. Sen, and U. Sen, Adv. Phys. **56**, 243 (2007).

[76] I. Bloch, J. Dalibard, and W. Zwerger, Rev. Mod. Phys. **80**, 885 (2008).

[77] J. Dalibard, F. Gerbier, G. Juzeliūnas, and P. Öhberg, Rev. Mod. Phys. **83**, 1523 (2011).

[78] A. Eckardt, Rev. Mod. Phys. **89**, 011004 (2017).

[79] G. Fano, F. Ortolani, and E. Colombo, Phys. Rev. B **34**, 2670 (1986).

[80] G. J. Sreejith, Y. Zhang, and J. K. Jain, Phys. Rev. B **96**, 125149 (2017).

[81] I. Dimov, B. I. Halperin, and C. Nayak, Phys. Rev. Lett. **100**, 126804 (2008).

[82] J. Biddle, M. R. Peterson, and S. Das Sarma, Phys. Rev. B **87**, 235134 (2013).

[83] M. Stern, P. Plochocka, V. Umansky, D. K. Maude, M. Potemski, and I. Bar-Joseph, Phys. Rev. Lett. **105**, 096801 (2010).

[84] T. D. Rhone, J. Yan, Y. Gallais, A. Pinczuk, L. Pfeiffer, and K. West, Phys. Rev. Lett. **106**, 196805 (2011).

[85] L. Tiemann, G. Gamez, N. Kumada, and K. Muraki, Science **335**, 828 (2012).